


An empirical model for the vertical-to-horizontal spectral ratios for Italy

Fadel Ramadan¹ | Chiara Smerzini²  | Giovanni Lanzano¹ | Francesca Pacor¹

¹ Istituto Nazionale di Geofisica e Vulcanologia (INGV), Milano, Italy

² Department of Civil and Environmental Engineering, Politecnico di Milano, Milano, Italy

Correspondence

Chiara Smerzini, Department of Civil and Environmental Engineering, Politecnico di Milano, Piazza Leonardo da Vinci 32 – 20133, Milano, Italy.

Email: chiara.smerzini@polimi.it

Funding information

DPC-ReLUIIS Project WP18 “Normative contributions related to seismic action”; INGV-DPC agreement B1 2019–2021

Abstract

This work presents a novel empirical Ground Motion prediction Model (GMM) for vertical-to-horizontal (VH) response spectral amplitudes up to 10 s, peak ground acceleration and velocity for shallow crustal earthquakes in Italy. Being calibrated on the most up-to-date strong motion dataset for Italian crustal earthquakes (ITA18), the model is consistent with the ITA18 GMM for the horizontal ground motion. This property makes the model useful in probabilistic seismic hazard assessment for Italy to derive compatible vertical and horizontal response spectra. To account for the increase of VH ratios in the proximity of the seismic source, an adjustment term is introduced to improve the prediction capability of the model in near-source conditions, relying on the worldwide NEar-Source Strong motion dataset (NESS). The proposed model uses a simple functional form restricted to a limited number of predictor variables, namely, magnitude, source-to-site distance, focal mechanism, and site effects, and the variability associated with both VH and V models is provided.

KEYWORDS

ground motion model, Italian crustal earthquakes, near-source effects, vertical-to-horizontal spectral ratios

1 | INTRODUCTION

For ordinary structures, seismic actions for design are typically prescribed only in terms of horizontal ground motion components, represented by a design response spectrum. According to the Italian Building Code - NTC18¹ and Eurocode 8 - EC8,² the vertical component of the seismic action shall be taken into account in a very limited number of cases, typically, for base-isolated structures and for selected building components (e.g. horizontal structural members with large spans). Nonetheless, it has been recognized that the vertical ground motion may be significantly larger than its horizontal counterpart in the near-source region of earthquakes, especially at periods less than about 0.3s, with potential impact for short-period structures.³ The relevance of the vertical ground motion has been clearly documented by the recent 2012 Po Plain (northern Italy) and the 2016 Central Italy seismic sequences.^{4,5} As an example, some stations located on the surface projection of the faults causative of the Norcia (30/10/2016, moment magnitude M_w 6.5) and the Po Plain (29/12/2012, moment magnitude M_w 6.0) earthquakes recorded maximum ratios of Vertical-to-Horizontal (VH) response spectral accelerations (SA) as high as about 3 and 8, respectively (see Figure 1), at short periods.

This is an open access article under the terms of the [Creative Commons Attribution-NonCommercial-NoDerivs](https://creativecommons.org/licenses/by-nc-nd/4.0/) License, which permits use and distribution in any medium, provided the original work is properly cited, the use is non-commercial and no modifications or adaptations are made.

© 2021 The Authors. *Earthquake Engineering & Structural Dynamics* published by John Wiley & Sons Ltd.

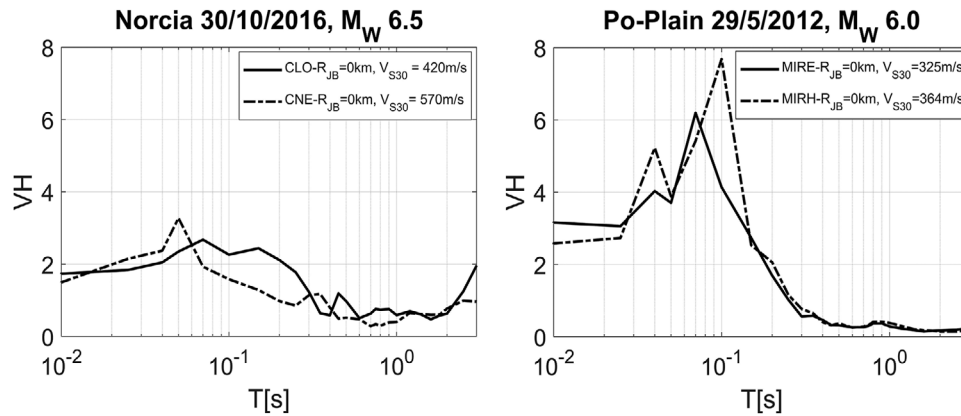


FIGURE 1 Vertical-to-Horizontal (VH) ratios of spectral acceleration (SA) at some near-source stations (CLO: Castelluccio di Norcia; CNE: Castel Sant'Angelo sul Nera; MIRE and MIRH: Mirandola) during the Norcia (30/10/2016, M_w 6.5, left) and Po-Plain (29/05/2012, M_w 6.0, right) earthquakes. Detailed information regarding the stations is available at the ITACA website: <http://itaca.mi.ingv.it/>

In such conditions, ignoring the vertical component may result in unsafe design assessments for special structures, such as low-rise buildings, masonry constructions, and long-span bridges.⁶ Vertical ground motion may play a crucial role for unreinforced masonry constructions, prominent in countries such as Italy, whose dynamic behavior is essentially governed by friction. As shown in Liberatore et al.,⁷ for these constructions, cycles of increments of axial loads can induce repetitive reductions of friction force, leading, therefore, to more extensive failures in small-cohesion structures. This finding is also supported by Di Michele et al.⁸ who concluded that fluctuations in the axial load strongly affect the flexural and shear capacity of masonry walls and a higher incidence of such effects is found for near-source records of large magnitude events. There are also evidences of the detrimental effect of vertical ground motion on Reinforced Concrete (RC) precast/frame structures^{9,10} as well as on bridge structures.^{11,12}

The considerations above have motivated our research focused on the characterization of vertical ground motion for engineering aims. In general, two main approaches can be used to develop vertical design seismic spectra in the framework of a Probabilistic Seismic Hazard Assessment (PSHA): (1) perform hazard integrations using Ground Motion Models (GMM) specifically developed for the vertical response spectral ordinates,^{13–16} separately from those for the horizontal components; (2) use a GMM for the VH response spectral acceleration ratios to scale the horizontal Uniform Hazard Spectrum (UHS). The main limitation of the first approach is that disaggregation of hazard may lead to different earthquake scenarios controlling the horizontal and vertical spectral accelerations. Such inconsistency may pose obstacles to site-specific engineering studies, such as in the selection of hazard-consistent three-component ground motions to be used in dynamic time history analyses of structures. For these reasons, the most commonly used approach is to generate the vertical spectrum by making use of empirical models for VH ratios.^{17–26} This approach, although simplified, is effective for seismic design purposes because it avoids performing vector-valued PSHA²⁷ including both horizontal and vertical components and the full treatment of their correlation.

The main aim of this study is to develop an empirical GMM for VH ratios of SA, Peak Ground Acceleration (PGA) and Peak Ground Velocity (PGV) for Italian shallow crustal earthquakes. The regression is calibrated using the strong motion dataset specifically developed for Italy, named ITA18, to update the GMM by Lanzano et al.²⁸ for the horizontal components. To account for the amplification of VH spectral ratios typically found in the proximity of the earthquake source, an adjustment factor is proposed to improve the median predictions and to avoid unsafe predictions when near-source scenarios control the hazard at the site. Following the Referenced Empirical Approach,^{29,30} this factor is calibrated from the residual analysis of the reference GMM (i.e., calibrated using the ITA18 dataset) with respect to the worldwide NEar-Source Strong motion dataset (NESS1.0).³¹ The proposed VH model is compatible with the horizontal GMM by Lanzano et al.,²⁸ because the dataset, record processing and functional form are common to both models. Figure 2 shows the conceptual framework at the basis of the methodology proposed to develop the Italian VH GMM adjusted for capturing the increase of vertical spectral demand in near-source conditions.

2 | VH SPECTRA FROM SEISMIC NORMS

Most of the seismic norms allow to design conventional structures only for the horizontal seismic actions and prescribe to consider the vertical excitation only in very limited cases. Specifically, according to EC8 – Part 1,² the new draft of

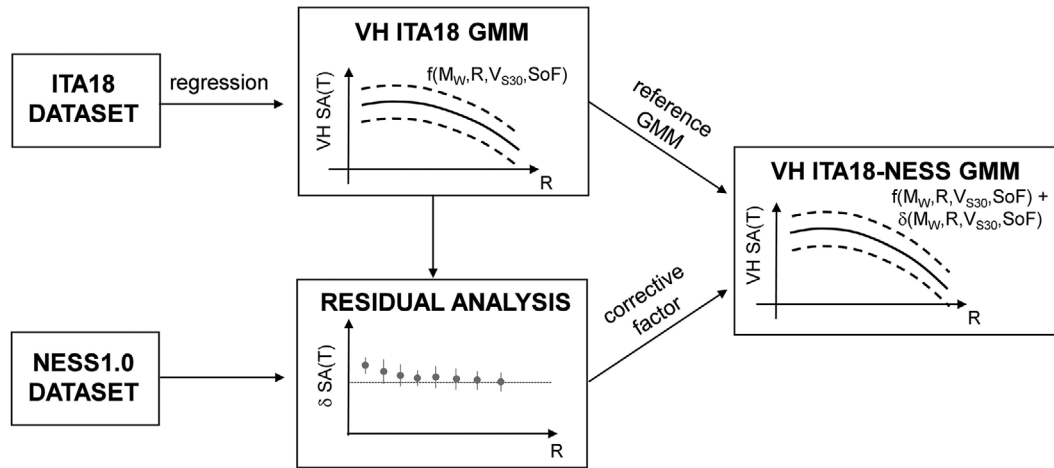


FIGURE 2 Flowchart of the methodology adopted for the empirical estimation of VH ground motion model

Eurocode 8³² and the NTC18,¹ these include specific structural members and structures, i.e., horizontal and nearly horizontal structural spanning members more than 20 m, horizontal and nearly horizontal cantilever component more than 5 m, horizontal pre-stressed components, beams supporting columns, and base-isolated structures. Furthermore, in some codes, further requirements are given in terms of exceedance of threshold values of vertical peak ground acceleration ($PGA_v > 0.25g$ for EC8) or maximum spectral acceleration ($S_{\alpha v} \geq 6.25 \text{ m/s}^2$ for EC8-Draft).

Historically, the simplest approach to derive vertical design spectra was to scale the horizontal spectrum by applying a period-independent factor equal to two-thirds (2/3). The Regulatory Guide (RG) 1.60³³ was one of the earliest guidelines to provide a design model for the VH spectral ratios, which is set equal to 2/3 for frequencies less than 0.25 Hz but equal to 1.0 for frequencies above 3.5 Hz.

In the last 30 years, it has been acknowledged that horizontal and vertical ground motions differ in the spectral content, magnitude scaling, attenuation rate with distance and site response. For these reasons, the VH ratio is sensitive to spectral period, distance from the source, magnitude and local site conditions and it is characterized by a distinct peak at short periods that typically exceeds 2/3 in the near-source region of an earthquake. These findings have been incorporated in recent seismic codes, such as EC8, the U.S. Building Code,^{34,35} the Turkish building code³⁶ and the EC8-Draft, where the vertical design spectrum is defined in a way which reflects more realistically the variation of the VH ratio with period (see overview in Kale and Akkar).³⁷ EC8 was one of the first code to introduce a vertical design spectrum and it was mainly based on the studies by Elnashai and Papazoglou.³⁸

The ASCE/SEI 7-16 norm in force accepts the 2009 NEHRP provisions,³⁹ which are mainly based on the work by Bozorgnia and Campbell.²⁴ However, the 2020 NEHRP provisions, which are expected to be incorporated into ASCE/SEI 7-22, recommends a revised definition of the vertical design spectrum to approximately match the VH spectral ratios from recent NGA-West 2 models.^{13,15,17,40} The definition of the vertical spectrum was revised in the EC8-Draft, by defining VH ratios variable with period and with ground motion intensity, consistently with the most recent empirical studies.²⁰

The New Zealand norm NZS 1170.5⁴¹ prescribes a simple period-independent VH ratio of 0.7. However, it recognizes, at least qualitatively, that the vertical component may be comparable to the horizontal one at short distances of 10 km or less from the seismic fault, where VH ratio should be considered as one for short periods $T \leq 0.3 \text{ s}$.

Figure 3 compares the VH spectra embedded in different international seismic codes, namely, EC8, EC8-Draft, NTC18, ASCE/SEI 7-16, NEHRP 2020, TBEC18 and NZS 1170.5, for both rock (left) and soft (right) sites. Note that the VH spectra are obtained by dividing the vertical design spectrum by the horizontal one, assuming a high seismicity arbitrary site. Rock and soft sites refer to ground type A and C for the European and Italian norms and to type B and D for the Turkish and U.S. standards. Detailed information on the most relevant parameters adopted in each seismic norm to define the vertical design spectrum is reported in Table A.1 of the Appendix. In the same table the base hazard parameters selected for the comparison of Figure 3 are provided.

At short periods ($T < 0.1\text{s}$), on rock sites, all norms tend to have similar VH ratios, except for EC8 which overestimates significantly the VH peak giving a ratio of 1.8. On soft soil sites, especially at shorter periods ($T < 0.2 \text{ s}$), the

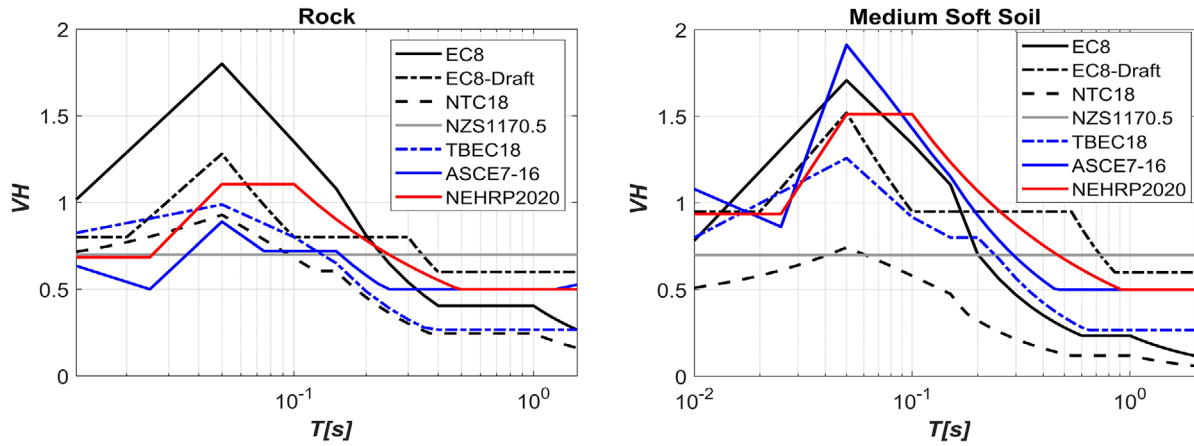


FIGURE 3 Design VH spectral ratios obtained from EC8 (Type 1), EC8-Draft, NTC18, ASCE/SEI 7–16, NEHRP 2020, TBEC18 and NZS1170.5 norms for rock (left) and soft soil (right) site. See Table A.1 in the Appendix for further details

variability of design VH ratios is much higher, with peak VH ratios ranging from 0.7 (NTC18) to about 2 (ASCE/SEI 7–16). It is noted that, contrary to other norms, EC8 and NTC18 prescribe VH ratios which are more conservative for rock than for soft sites. This is due to the different way through which site conditions are accounted for in the definition of the vertical design spectra. Specifically, in EC8, the local site conditions do not enter directly in the definition of the vertical design spectrum. The latter is, in fact, anchored on the PGA_v estimated as a fraction of the reference horizontal PGA, equal to either 90% (Type 1 spectrum) or 45% (Type 2), depending on the seismicity of the area (for high and low seismicity, respectively), and it has constant corner periods regardless of the site conditions. A similar rationale is behind the NTC18, where the vertical design spectrum is a function of the maximum vertical spectral amplification factor, F_v , which is defined as a non-linear increasing function of PGA. On the other hand, in U.S. provisions, a vertical coefficient, C_v , is defined to account for the dependence of the VH ratios on the site class and on the seismicity of the area. In EC8-Draft, site classes are indirectly taken into account in the definition of the vertical spectrum, because of the scaling of the site-dependent horizontal spectrum. The comparison between ASCE/SEI 7–16 and 2020 NEHRP provisions highlights two main aspects: first, the revised spectral shape somehow regularizes the VH ratios recommended previously, providing a lower constant value in the range of periods between 0.025 and 0.05 s; second, the decay with period of the vertical design spectrum in the mid-period part has been updated from $T^{-0.75}$ to $T^{-0.5}$.

3 | EMPIRICAL MODELS FOR VH RATIOS

In literature, several models, the major of them empirically developed, are available to predict the VH ratios in regions of shallow crustal seismicity. In this study four recent models are considered, namely, BC2016,¹⁷ GA2011,²⁰ BO2011¹⁹ and AK2014.¹⁸

Table 1 provides an overview of the aforementioned empirical models, along with the model proposed in this study, with indication of the main features of the predictive relationships in terms of reference dataset, tectonic context, range of M_w and of source-to-site distance, explanatory variables and type of modeling for site response. With reference to the modelling of soil behavior, it is remarked that, while the BO2011 model accounts for linear ground response, a non-linear behavior is taken into account in GA2011 (only the horizontal component), AK2014 and BC2016 (both vertical and horizontal components).

Both BO2011 and AK2014 are suitable for predictions in Europe and Middle East (AK2014 updates the BO2011 model by making use of the RESORCE dataset consisting of 1041 recordings of M_w in the range from 4 to 8), while GA2011 and BC2016 are based on worldwide datasets including 2684 and 21332 recordings of $M_w = [5-8.5]$ and $[3.3-8.5]$, respectively. Although BO2011 is superseded by AK2014, we prefer to keep it for comparison purposes because, like our model, it does not introduce soil non-linearity into the modeling of site response.

TABLE 1 Main features of selected VH GMMs available in the literature

	BO2011	GA2011	AK2014	BC2016	This study
Dataset	Strong-motion database for Europe and Middle East: 1267 records from 392 events	Subset of the PEER-NGA worldwide database: 2684 recordings from 127 worldwide events	Subset of the RESORCE database for Europe and Middle East: 1041 records from 221 events.	NGA-West2 worldwide ground motion database: 21'332 records from 599 events.	ITA18 dataset for Italy: 5778 records from 156 events
Tectonic context	Shallow crustal seismicity (Europe and Middle East)	Shallow crustal seismicity (worldwide)	Shallow crustal seismicity (Europe and Middle East)	Shallow crustal seismicity (worldwide)	Shallow crustal seismicity (Italy)
M_w	[4.5-7.6]	[5.0-8.5] for strike-slip [5.0-8.0] for dip-slip	[4.0-8.0]	[3.3-8.5]	[3.5-7.5]
Source-to-Distance	R_{JB} ¹ up to 100 km	R_{rup} ³ up to 200 km	R_{JB} up to 200 km	R_{rup} up to 300 km	R_{rup} or R_{JB} up to 200 km
Intensity measures	PGA, SA(0.02-3s)	PGA, PGV, SA(0.01-10s)	PGA, PGV, SA(0.01-4s)	PGA, PGV, SA(0.01-10s)	PGA, PGV, SA(0.01-10s)
Explanatory variables	M_w, R_{JB}, SoF^2 , Site class	M_w, R_{rup}, SoF & V_{S30} ⁴	M_w, R_{rup}, SoF & V_{S30}	$M_w, R_{rup}, R_{JB}, R_X^5, Z_{tor}^6, \delta^7, SoF, V_{S30}, Z_{2.5}^8$ & Z_{hyp}^9 .	M_w, R_{rup}, SoF & V_{S30}
Soil behavior	Linear function	Non-linear function for H and linear for V	Non-linear function for both H and V	Non-linear function for both H and V	Linear function

R_{JB} ¹: Joyner-Boore distance; SoF ²: Style of faulting; R_{rup} ³: rupture distance; V_{S30} ⁴: time-averaged shear-wave velocity in the top 30 m; R_X^5 : closest distance to the surface projection of the top edge of the co-seismic fault rupture plane measured perpendicular to its average strike; Z_{tor} ⁶: depth to the top of the fault rupture plane; δ^7 : average dip angle of the fault rupture plane measured from a horizontal plane; $Z_{2.5}^8$: depth to the 2.5 km/s shear-wave velocity horizon beneath the site; Z_{hyp} ⁹: hypocentral depth of the earthquake measured from sea level.

4 | THE DATASET: ITA18

The VH GMM model calibrated in this study is based on the ITA18 dataset, built to develop the horizontal GMM by Lanzano et al.²⁸ for shallow active crustal regions in Italy. This dataset is composed of 5778 strong-motion records for 156 events in which about 90% are representative of Italian seismicity. The M_w ranges between 3.5 and 8 and records are selected from 1684 stations within a R_{JB} up to 200 km (see Figure 4). Besides, the events are classified with normal (NF, 47% of total events), reverse (TF, 28%) and strike-slip (SS, 25%) focal mechanisms. We refer the reader to Lanzano et al.²⁸ for detailed information regarding the dataset processing.

In our analysis, at each period T , the VH ratio is computed by dividing the vertical SA(T) by the horizontal RotD50 component, defined as the median of the distribution of the SA, obtained from the combination of the two horizontal components across all non-redundant azimuths.⁴² The observed trends of VH ratios are shown as a function of some explanatory variables, such as magnitude and the source-to-site-distance, introduced by both the rupture distance R_{rup} and the Joyner and Boore distance R_{JB} . These metrics are available for all the events with $M_w > 5.5$ for which the geometry of the fault is known; when not available, the epicentral distance (R_{epi}) is regarded equivalent to R_{JB} , and the hypocentral distance (R_{hyp}) to R_{rup} .

Figure 5 shows the empirical cumulative frequency distributions of VH ratios of SA (0.1s) and SA (1s) computed from the entire ITA18 dataset. As expected, for a given fractile, higher amplitudes are found for short period spectral accelerations: specifically, about 2% of ITA18 records has VH ratios at 0.1 s and 1.0 s exceeding 1.7 and 1.4, respectively. Furthermore, it is found that about 15% of records has VH ratios at 0.1 s larger than 1.

Figure 6 shows the trends of the median VH ratios of the ITA18 dataset for two periods ($T = 0.1$ s, left; $T = 1$ s, right) as a function of R_{JB} and M_w . The median values are computed by grouping the VH observations in equally spaced distance and

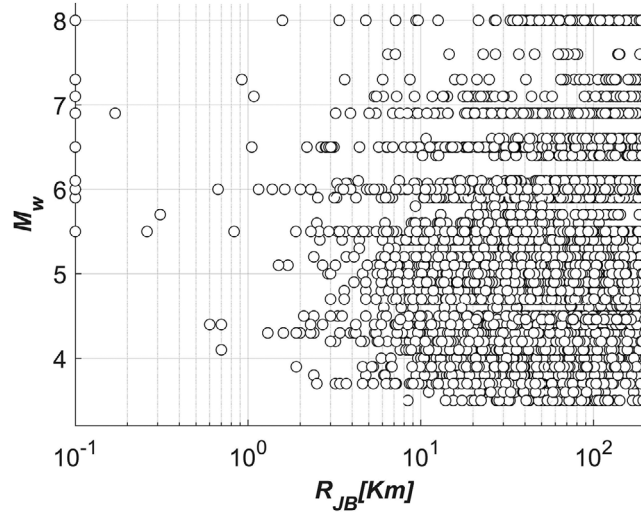


FIGURE 4 M_w - R_{JB} distribution of ITA18 dataset, after Lanzano et al.³²

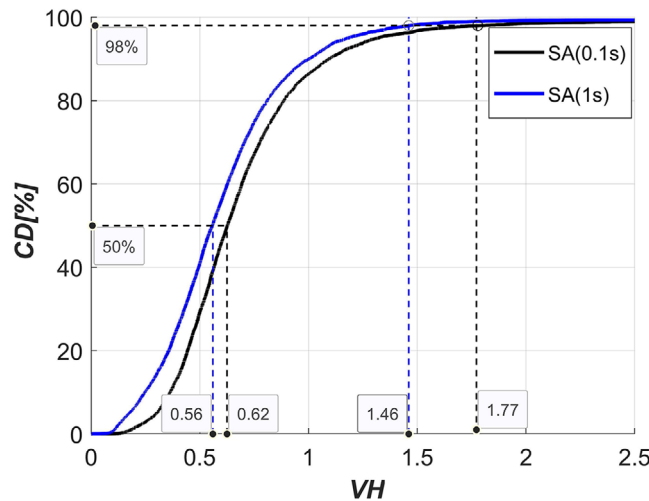


FIGURE 5 Cumulative frequency distribution (CD) of observed VH ratios of both SA(0.1s) and SA(1s) from ITA18 dataset

magnitude bins. The attenuation of short-period VH ratios with distance (Figure 6, top) is significant at distances within 30 km, especially for larger magnitude ranges; at longer periods, the VH ratios tend to increase mildly with distance, as also found by other authors.¹⁹ The observed VH ratios, as well as the rate of decay with distance, do not show a strong dependence on magnitude (Figure 6, bottom). The analysis of VH ratios also shows a limited dependence on soil condition (V_{S30}) and focal mechanism (not reported here for sake of brevity).

5 | CALIBRATION OF THE ITA18 VH MODEL

5.1 | Functional form

On the basis of the data analysis shown in the previous section, the functional form adopted for the VH ITA18 median model is defined as follows:

$$\log_{10} Y = a + F_M(M_W, SoF) + F_D(M_W, R) + F_S(V_{S30}) \quad (1)$$

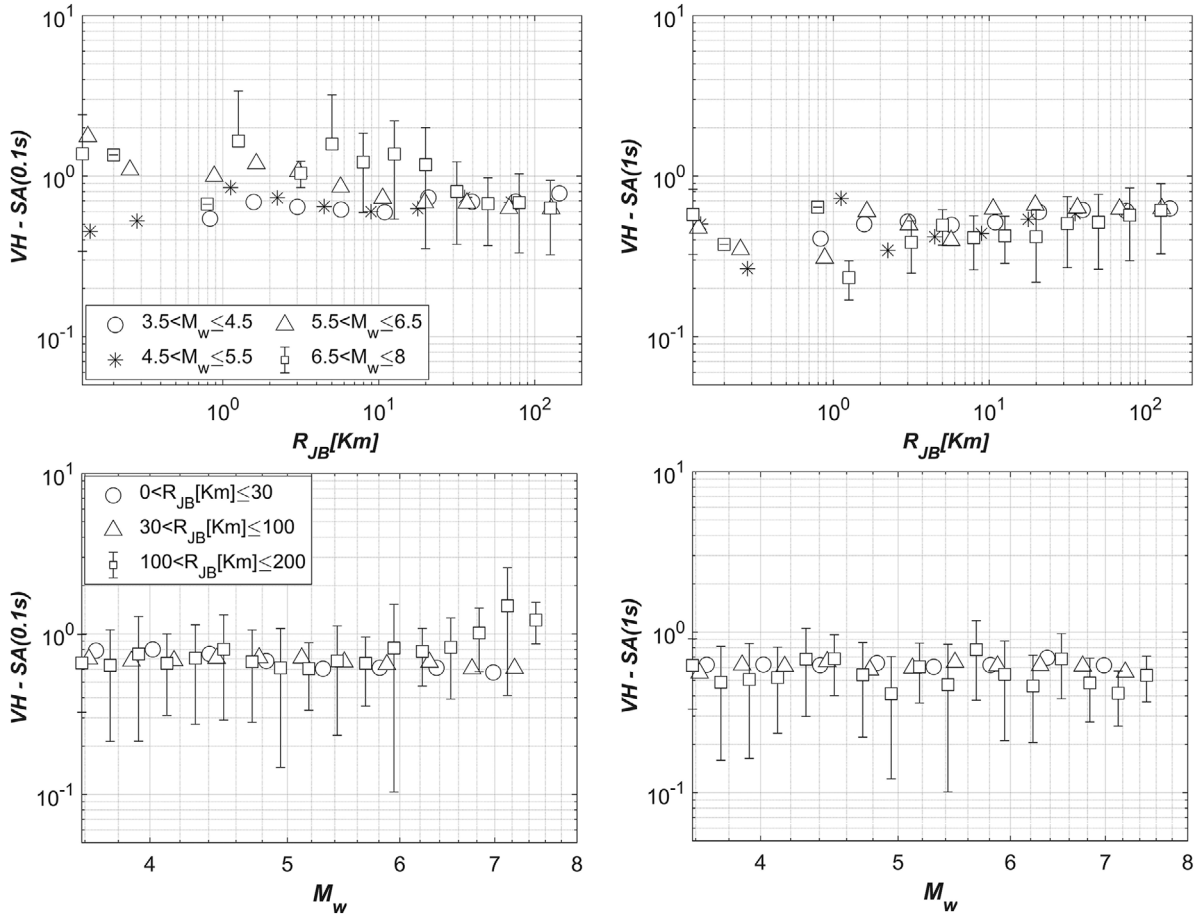


FIGURE 6 Attenuation with distance (top) and magnitude scaling (bottom) of median VH ratios from ITA18 dataset for SA(0.1s), left, and SA(1s), right. Dispersion bands are shown only for selected bins

where Y is the VH ratios for PGA, PGV and 36 ordinates of the 5% damping acceleration response spectra (SA) in the period range 0.01-10 s, a is the offset, $F_M(M_W, SoF)$ is the source function, $F_D(M_W, R)$ is the distance function and $F_S(V_{S30})$ is the site term. The functional form is consistent with the one adopted for the horizontal GMM of Lanzano et al.,²⁸ apart from a minor modification regarding the source term owing to the more limited dependence of VH on M_W (herein the magnitude scaling is controlled by a simple linear function, whereas in Lanzano et al.²⁸ by a stepwise linear function). The almost negligible dependence on M_W indicates that the source scaling of the horizontal component is very similar to that of the vertical component. For the final regression, we decided however to keep the linear magnitude scaling term because some sensitivity tests indicated a lower dispersion. Specifically, the source term consists of two terms:

$$F_M(M_W, SoF) = bM_W + f_j SoF_j \quad (2)$$

where coefficient b controls the source scaling and the coefficients f_j provide the correction for the Style of Faulting (SoF) of the event. SoF_j s are dummy variables, introduced to specify strike-slip SS ($j = 1$), reverse TF ($j = 2$), and normal NF ($j = 3$) focal mechanism types. The regression is performed constraining to zero the coefficient for normal faulting ($f_3 = 0$). The path term is defined as:

$$F_D(M_W, R) = [c_1 (M - M_{ref}) + c_2] \log_{10} R \quad (3)$$

where the first term is the magnitude-dependent geometrical spreading and the second is the distance attenuation, M_{ref} is the reference magnitude assumed to be constant for all periods with a value of 6.0, while c_1 and c_2 are the path coefficients. The distance is computed as $R = \sqrt{R_{JB}^2 + h^2}$, in which R_{JB} is substituted by R_{rup} when using the model coefficients

related to R_{rup} , and h is the pseudo-depth, assumed to be constant for all periods with a value of 5 km. The values of $M_{ref} = 6$ and $h = 5$ km were calibrated from a first stage non-linear regression.

Finally, the site term is defined as a function of the time-averaged shear wave velocity in the top 30 meters (V_{S30}):

$$F_S(V_{S30}) = k \log_{10} \left(\frac{V_0}{800} \right) \quad (4)$$

in which $V_0 = V_{S30}$ when $V_{S30} \leq 1500$ m/s and $V_0 = 1500$ m/s otherwise. Because the record sampling of very hard-rock sites is poor, the upper bound of the V_{S30} scaling, above which the amplification is independent on this explanatory variable, corresponds to 1500 m/s according to Kamai et al.⁴³ The function is linearly dependent on V_{S30} , consistently with the ITA18 horizontal model. In particular, the non-linear site response term in horizontal GMM was neglected because there are insufficient records to robustly constrain these effects. Another strategy, followed in several works (GA2011; AK2014; BC2016) consists in calibrating the non-linear site scaling on the basis of numerical simulations; however, this approach tends to over-estimate the effects of the non-linearity, especially at short periods.^{44,45}

5.2 | Regression analysis

A linear ordinary least-squares mixed-effects regression method is used. The method is suggested by Bates et al.⁴⁶ and composed of fixed effects and random effects. The fixed effects are applied to evaluate the source (b), path (c_1 and c_2), and site term (k) coefficients and the random effects are applied to stations and events to perform the residual analysis and estimate the partially non-ergodic sigma according to.⁴⁷

Following the procedure of Lanzano et al.²⁸ and according to Wasserstein and Lazar,⁴⁸ the statistical significance of model coefficients (P-Values) is tested for each fixed coefficient. The smaller the P-Value is, the higher the possibility to reject a null hypothesis is. In other words, coefficients with low P-Values (< 0.05) are considered to be significant and meaningful to the model, instead, coefficients with high P-Values (> 0.05) are considered to be less significant and meaningful to the model.

The regression coefficients obtained considering both R_{rup} and R_{JB} are reported in the Electronic Supplement S1, while the Supplement S2 lists their corresponding P-Values at PGA, SA(0.1s) and SA(10s). It is noticeable that the site coefficient (k) assumes values close to zero at short periods (0.1s), but the P-Value is quite high (> 0.05). Consequently, the site effect seems to be not effectively modeled at SA (0.1s) and it is expected to obtain high site-to-site variability at that period. Furthermore, as for the horizontal model, SoF correction f_1 and f_2 mostly exhibit high P-Values, meaning that these terms are not a meaningful addition to our VH model.

5.3 | Residuals analysis

According to Rodriguez-Marek et al.,⁴⁹ total residuals (R_{es}), defined as the difference between observed ground motion parameters and the values predicted by the model (in log10 units), are separated into a between-event term (δB_e), site-to-site term ($\delta S2S_s$) and site- and event- corrected term (δWS_{es}):

$$R_{es} = \delta B_e + \delta S2S_s + \delta WS_{es} \quad (5)$$

where the subscripts denote an observation for event e at station s . The δB_e (also called inter-event residual or event term) represents the average shift of the observed ground motion of an individual earthquake, e , from the population median predicted by the GMM. The $\delta S2S_s$ represents the systematic deviation of the observed ground motion at site s (i.e., the site term) from the median event-corrected ground motion predicted by the model, and δWS_{es} is the site- and event-corrected residual.

Figure 7 shows the trend of δB_e , $\delta S2S_s$ and δWS_{es} residuals with respect to M_W , V_{S30} , and R_{JB} , respectively, for both SA(0.1s), left, and SA(1s), right. The δB_e error (Figure 7, top) is within the range of $[-0.1, 0.1]$ log 10 units, with no trend with magnitude. The $\delta S2S_s$ (Figure 7, center) is within the range of $[-0.5, 0.5]$ log 10 units with unbiased trend, especially in the range of V_{S30} containing the largest number of records (300-800 m/s). The figure shows that the $\delta S2S_s$ has higher variability compared to δB_e at both SA(0.1s) and SA(1s). This behavior is probably related to

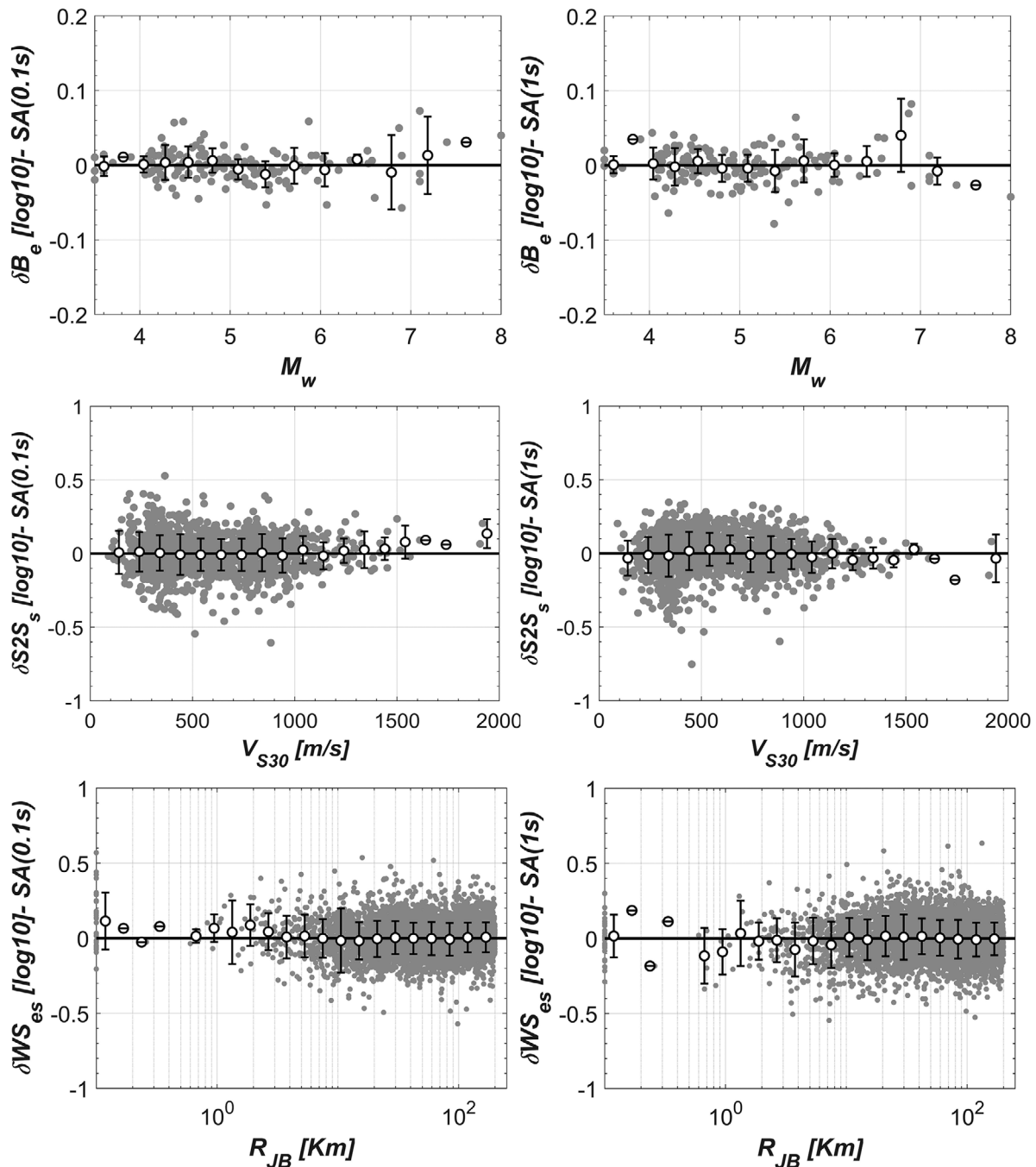


FIGURE 7 Residuals of the VH ITA18 for SA(0.1s), left, and SA(1s), right. Top: between-event residuals versus M_w ; center: site-to-site residuals versus V_{S30} ; bottom: event- and site-corrected residuals versus R_{JB}

two factors. First, the ITA18 dataset used is composed by more than 2/3 of the records from stations with V_{S30} estimated indirectly by an empirical correlation with the topographic slope⁵⁰ rather than being measured. The second factor could be related to the assumed functional form for the site term, prescribed only by a linear dependence on V_{S30} . As remarked by Laurendeau et al.,⁵¹ this short period variability should be explained through the use of the high-frequency attenuation parameter (i.e. the kappa term κ_0), as additional explanatory variable for GMMs calibration.

The δWS_{es} (Figure 7, bottom) shows unbiased trend with distance. However, as the dataset includes a limited number of records at short distances, the residuals at $T = 0.1s$ are relatively higher for $R_{JB} < 20$ km. The trend of δWS_{es} for soft soil sites ($V_{S30} \leq 360$ m/s) as a function of the horizontal PGA from Lanzano et al.²⁸ on rock ($V_{S30} = 800$ m/s) indicated a

limited influence of non-linear site response effects for high levels of shaking, thus corroborating our assumption of linear site response model (see Figure S3.1 in Supplement S3).

5.4 | Variability analysis of VH and V models

The total standard deviation σ_{VH} of the VH GMM is homoscedastic and is given by:

$$\sigma_{VH} = \sqrt{\tau_{VH}^2 + \psi_{VH}^2 + \phi_{VH}^2} \quad (6)$$

where τ_{VH} , ψ_{VH} and ϕ_{VH} are the standard deviations of the terms δB_e , $\delta S2S_s$ and δW_{es} , respectively.

Furthermore, as the model is consistent with the ITA18 horizontal GMM, the vertical ground motion can be assessed by adding the logarithmic prediction of VH ITA18 ratio to the logarithmic prediction of horizontal SA from Lanzano et al.,²⁸ as follows:

$$\log_{10} Y_V = \log_{10} Y_H + \log_{10} Y_{V,H} \quad (7)$$

As regards the variability treatment, the standard deviations of the predicted vertical ground motion are computed from the error propagation of the various components of the standard deviation, considering the correlation between VH and H random variables under the assumption that they are log-normally distributed,¹⁷ as:

Between-event variability

$$\tau_V = \sqrt{\tau_H^2 + \tau_{VH}^2 + 2\rho_{H,VH}^\tau \tau_H \tau_{VH}} \quad (8)$$

Site-to-site variability

$$\psi_V = \sqrt{\psi_H^2 + \psi_{VH}^2 + 2\rho_{H,VH}^\psi \psi_H \psi_{VH}} \quad (9)$$

Event- and site-corrected variability (remaining variability)

$$\phi_V = \sqrt{\phi_H^2 + \phi_{VH}^2 + 2\rho_{H,VH}^\phi \phi_H \phi_{VH}} \quad (10)$$

such that

$$\sigma_V = \sqrt{\tau_V^2 + \psi_V^2 + \phi_V^2} \quad (11)$$

where: H, V and VH belong to horizontal, vertical and vertical-to-horizontal components respectively; τ , ψ and ϕ are the various components of standard deviation as defined previously; $\rho_{H,VH}^\tau$, $\rho_{H,VH}^\psi$ and $\rho_{H,VH}^\phi$ are the correlation coefficients between H and VH components of δB_e , $\delta S2S_s$ and δW_{es} , respectively (provided in Supplement S1). A quantitative discussion on the model uncertainties will be addressed in the sequel, see Figure 11.

5.5 | Verification against observations from ITA18 dataset

In Figure 8 the predictions of vertical SA(0.1s), left, and SA(1.0s), right, from the ITA18 model are compared with the observations available for two magnitude levels ($M_W 4.0$ and $M_W 6.3$), for $V_{S30} = 450 \pm 100$ m/s and for different *SoF*. It is noted that, at both short and long periods, the observations (dots) are mostly included in the range of the empirical predictions (continuous line: median, dashed line: $\pm \sigma_V$). However, it is remarked that some discrepancies are observed at longer distances: the ITA18 model (both H and VH), in fact, cannot be considered properly “regional” since the seismic

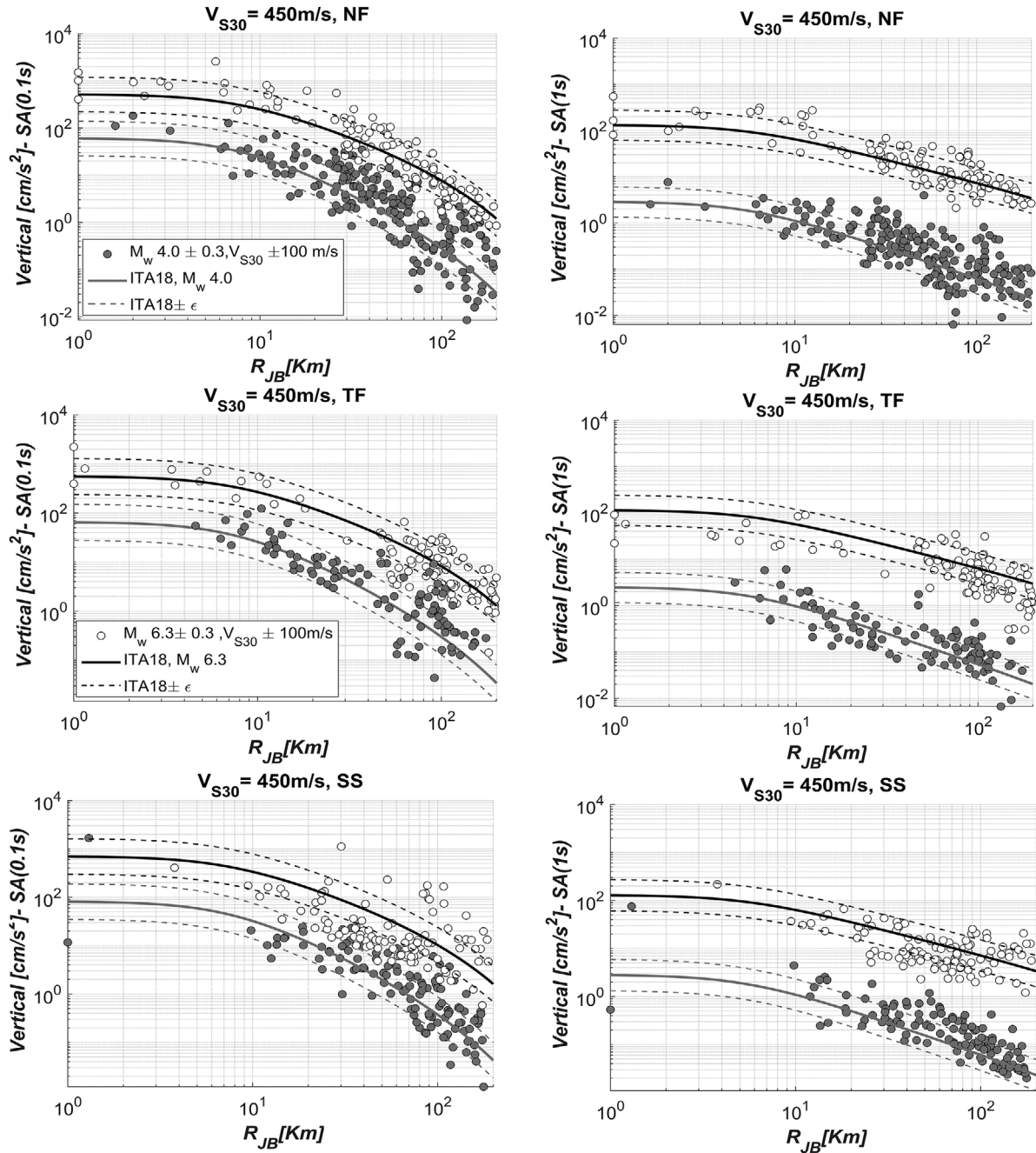


FIGURE 8 Median ($\pm \sigma$) vertical SA(0.1s), left, and SA(1s), right, as a function of R_{JB} , for $M_w 4.0$ and $M_w 6.3$ scenarios (top: NF; center: TF; bottom: SS) with $V_{S30} = 450 \text{ m/s}$, against observations from ITA18 dataset (superimposed dots, $V_{S30} \pm 100 \text{ m/s}$, $M_w \pm 0.3$)

wave propagation features affecting the anelastic attenuation are significantly different among regions in Italy. Our model captures an average attenuation, being slightly conditioned by the characteristics of the propagation medium in Central Italy, where most events of the ITA18 dataset are located.

In addition, at $T = 0.1\text{s}$, the empirical model tends to underestimate the data at very short distances (less than $R_{JB} < 10 \text{ km}$), especially for larger magnitude events. As an illustrative example, Figure 9 shows the comparison between the predicted and observed median VH ratios for a near-source $M_w = 6.3$ scenario (normal fault) on stiff soil. The bias of empirical predictions is apparent, with maximum underpredictions of about 40%, and it is related to the low proportion of near-fault records in the ITA18, which makes the prediction poorly constrained at short distances.

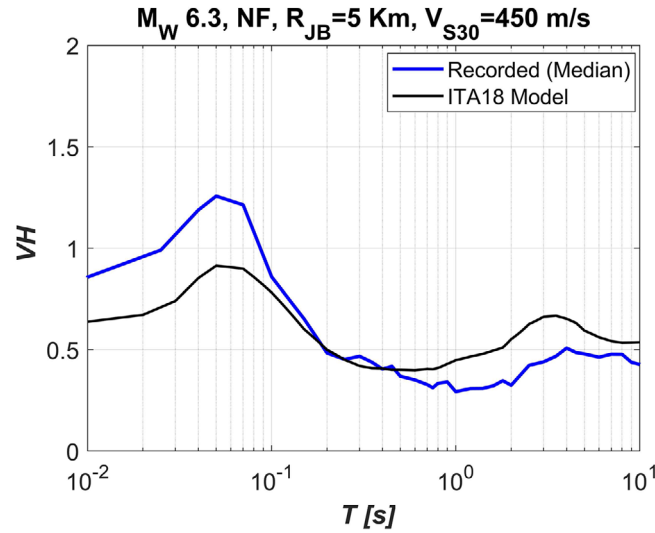


FIGURE 9 Comparison between recorded and predicted median VH spectral ratios for a near-source earthquake scenario with M_W 6.3 (± 0.3 for records), NF, $R_{JB} = 5$ km (± 5 km) and $V_{S30} = 450$ m/s (± 100 m/s)

This observation motivated our decision to introduce in the GMM an adjustment factor on the median ITA18 predictions in near-source conditions, as described in the following section.

6 | ADJUSTMENT FOR NEAR-SOURCE EFFECTS

As commented previously, regional datasets, such as the Italian one, are mainly governed by far-field recordings and this may produce biases in ground motion prediction in the proximity of the seismic source. The objective of this section is, therefore, to propose a simplified approach to improve the median predictions of the ITA18 model in near-source conditions, which are known to generally control the seismic hazard in Italy. Although more sophisticated approaches should be grounded on the modeling and parameterization of near-source physical processes (e.g. forward directivity, hanging-wall/footwall effects), we preferred calibrating a near-source factor to adjust the ITA18 predictions because of the inherent issues related to the calibration of complex functional forms and to their use in practical applications. Following the Referenced Empirical Approach,^{29,30} a near-source factor (F_{ns}) is proposed for the reference GMM (i.e. the GMM calibrated on ITA18), based on the residual analysis of the reference GMM with respect to an independent dataset specifically developed for near-source ground motions. In particular, F_{ns} has been calibrated using the NESS1.0 dataset, a worldwide strong-motion dataset including only high-quality recordings obtained in near-source conditions,³¹ see <http://ness.mi.ingv.it/>. NESS1.0 consists of about 800 three-component waveforms relative to 700 accelerometric stations, caused by 74 crustal earthquakes with $M_W \geq 5.5$ and R_{JB} up to 140 km. The Italian strong-motion data recorded in near-source region are also archived in the NESS1.0.

6.1 | Functional form for the near-source factor F_{ns}

The near-source factor is determined by fitting the residuals of ITA18 with respect to NESS1.0 data using a suitable functional form. The ITA18-NESS residuals are computed as follows:

$$\delta_C = \log_{10}(VH_{OBS,NESS}) - \log_{10}(VH_{ITA18}) \quad (12)$$

where $VH_{OBS,NESS}$ represents the observed VH from NESS1.0 dataset and VH_{ITA18} represents the predicted ratios from the ITA18 model as in Equation (1).

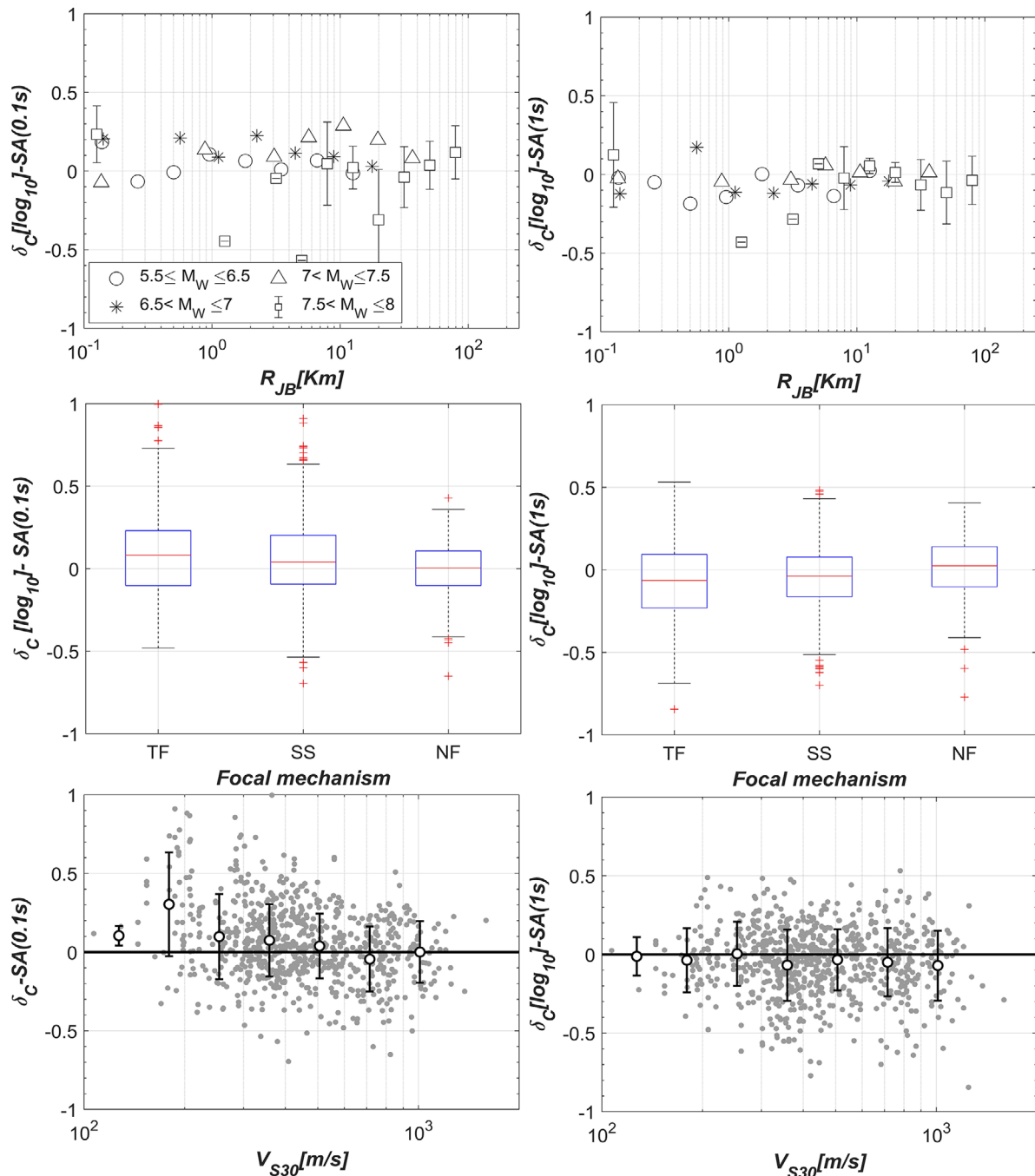


FIGURE 10 Residuals, see Equation (12), with respect to R_{JB} (top), SoF (center), and V_{S30} (bottom), for SA(0.1s), left, and SA(1s), right

Figure 10 shows δ_C as a function of R_{JB} , V_{S30} and focal mechanism. At short periods (0.1s, left), the dependence of the residuals on the R_{JB} , V_{S30} (top and bottom) and M_W (not reported here) is noticeable, and it is more pronounced for SS and TF faults (center), whereas, at long period (1s, right), the residuals have an overall lower variability.

Based on these results, the regression function for the residuals is defined as follows:

$$\hat{\delta}_C = a_R + F_{MR}(M_W, SoF) + F_{DR}(R) + F_{SR}(V_{S30}) \quad (13)$$

where a_R is the offset, $F_{MR}(M_W, SoF)$ is the source function, $F_{DR}(R)$ is the distance function, and $F_{SR}(V_{S30})$ is the site term:

$$F_{MR}(M_W, SoF) = b_R M_W + f_{jR} SoF_j \quad (14)$$

$$F_{DR}(R) = c_R \log_{10} R \quad (15)$$

$$F_{SR}(V_{S30}) = k_R \log_{10} \left(\frac{V_0}{800} \right) \quad (16)$$

The coefficients, b_R , f_{jR} , c_R , and k_R , and variables R , M_W and V_0 definitions follow the VH ITA18 model. However, the pseudo depth used herein is $h_R = 1$ km, obtained from some trial regressions.

Applying the same regression method described previously, we computed the regression coefficients (Electronic Supplement S1) and the corresponding P-values (Electronic Supplement S2). Apart from the focal mechanism coefficients, other coefficients are statistically meaningful at short periods. In particular, and differently from the VH ITA18 model, the soil term coefficient, k_R , has low P-Values (< 0.05) at both short and long periods.

Therefore, an adjusted VH model, referred to as VH ITA18-NESS hereafter, is proposed as follows:

$$\log_{10} VH_{ITA18-NESS} = \log_{10} VH_{ITA18} + F_{ns} \text{ with } F_{ns} = \max(\hat{\delta}_C, 0) \quad (17)$$

Note that F_{ns} is set to zero when negative. This reflects the rationale behind the ITA18-NESS model: our aim is to improve the baseline regional GMM by adjusting its median estimates and, hence, limiting possible unsafe biases in near-source conditions.

6.2 | Model variability

The total variability of the ITA18-NESS model is simply estimated as the standard deviation of the residuals between the logarithmic VH predictions and observations included in the reference ITA18 dataset. Accordingly, the total standard deviation has been decomposed into the various components (τ , ψ and ϕ) and the propagation of errors (see Equations (8)–(11)) is applied to compute the variability of V predictions of the VH ITA18-NESS. Standard deviations and correlation coefficients of ITA18-NESS model are reported in Supplement S1.

Figure 11 shows the different terms of standard deviation for V, H and VH components for both ITA18 and ITA18-NESS model. For comparison purposes, the total standard deviation of BO2011 is also shown. Referring to the VH models, the between-event variability (τ) contributes marginally to the total variability, being below 0.1 in log10 units, because, as expected, the between-event terms of vertical and horizontal ground motion components (which are correlated) cancel each other, yielding an overall reduction of the between-event variability of the VH model [see also Bommer et al.¹⁹].

The main contribution to the VH variability comes from the site-to-site variability (ψ), owing to the large uncertainties associated with the adopted model for site response. As a matter of fact, the inclusion of high-frequency attenuation term and non-linear soil behavior may contribute to decrease the standard deviation.

Looking at the trend of the total variability of the VH model (σ), a slight increase is found from PGA to SA(0.1s), where σ reaches a maximum value of nearly 0.4. After around 0.6 s, σ tends to reach a constant value of around 0.3 independently on the period. These results are in substantial agreement with BO2011. Furthermore, Figure 11 points out that the variability components obtained for V and H models have comparable values, reflecting the consistency of the VH ratio model with the reference horizontal model by Lanzano et al.²⁸

The variabilities of the ITA18-NESS models are generally slightly larger than the corresponding ones of ITA18. This is expected, since ITA18-NESS does not correspond to the best fitting model against ITA18 dataset and, hence, to the minimum variability. In essence, we should gain greater predictive power, paying the price of a small increase in standard deviation.

The verification against NESS data is addressed in Figure S3.2 of the Electronic Supplement S3, where the predictions of vertical SA(0.1s) from both the ITA18-NESS and ITA18 models are compared with the NESS recordings for two magnitude

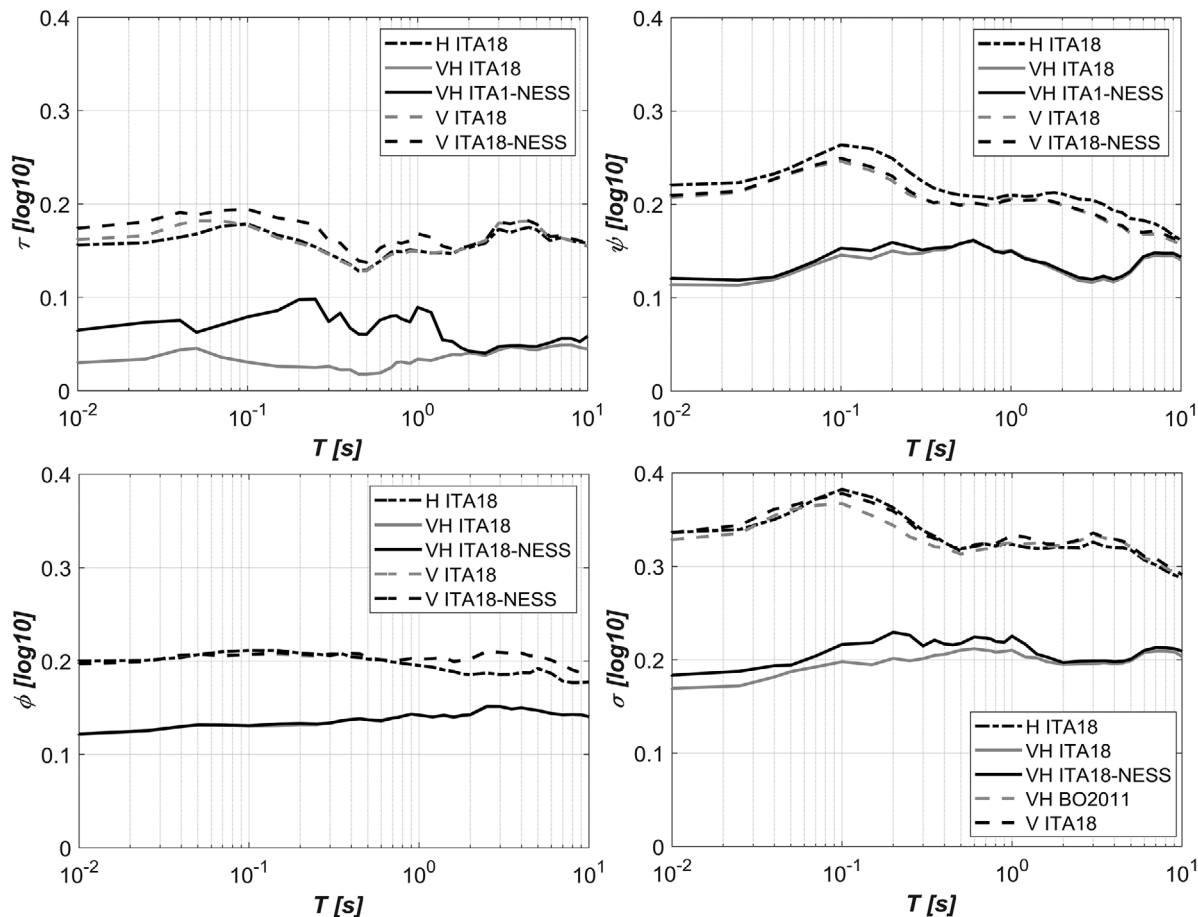


FIGURE 11 Between-event (τ), site-to-site (ψ), event- and site-corrected (ϕ) and total (σ) standard deviation for V, H and VH predictions. The σ values from BO2011 are also shown for comparison

levels ($M_w 6.0$ and $M_w 7.0$), for rock and stiff sites ($V_{S30} = 700 \pm 100$ m/s; $V_{S30} = 400 \pm 100$ m/s) and for different SoF . The site conditions are selected to get an appreciable number of records in the NESS1.0 dataset. As the residuals at long periods are negative (so that the correction factor is null), only the spectral ordinate at 0.1s is shown, for which the ITA18-NESS yields to an amplification of the ITA18 model.

It is apparent that the adjusted model (ITA18-NESS) amplifies the ITA18 predictions especially at R_{JB} less than about 10 km, while at larger distances the correction term tends to be very limited. Such an increase is higher for larger magnitude events. The introduction of F_{ns} turns out to have a negligible effect for NF events, while it is relevant for TF and SS. With respect to soil condition (V_{S30}), the improvement is rather clear leading to higher vertical motions for lower V_{S30} in the ITA18-NESS model.

The comparison with NESS observations improves with the ITA18-NESS model, thus overcoming the bias previously noted for the ITA18 model at near-source sites. Nevertheless, for TF and $V_{S30} = 300$ m/s, and for $M_w 6.0$, an underestimation is still found, most likely because the H ITA18 model could underestimate the observations in near source conditions for some scenarios, as for the VH ITA18 model.

7 | MEDIAN VH RATIOS OF THE PROPOSED MODELS

Figure 12 shows the median VH spectra of the proposed ITA18 and ITA18-NESS models for different scenario earthquakes, obtained by varying the explanatory variables one at a time (Figure 12A: R_{JB} ; Figure 12B: M_w ; Figure 12C: SoF ; Figure 12D: V_{S30}). At short periods (less than 0.1 s), as expected, the VH ratios show a strong dependence on distance (Figure 12A), with higher values, up to nearly 1.5, for near-source sites (< 15 km).

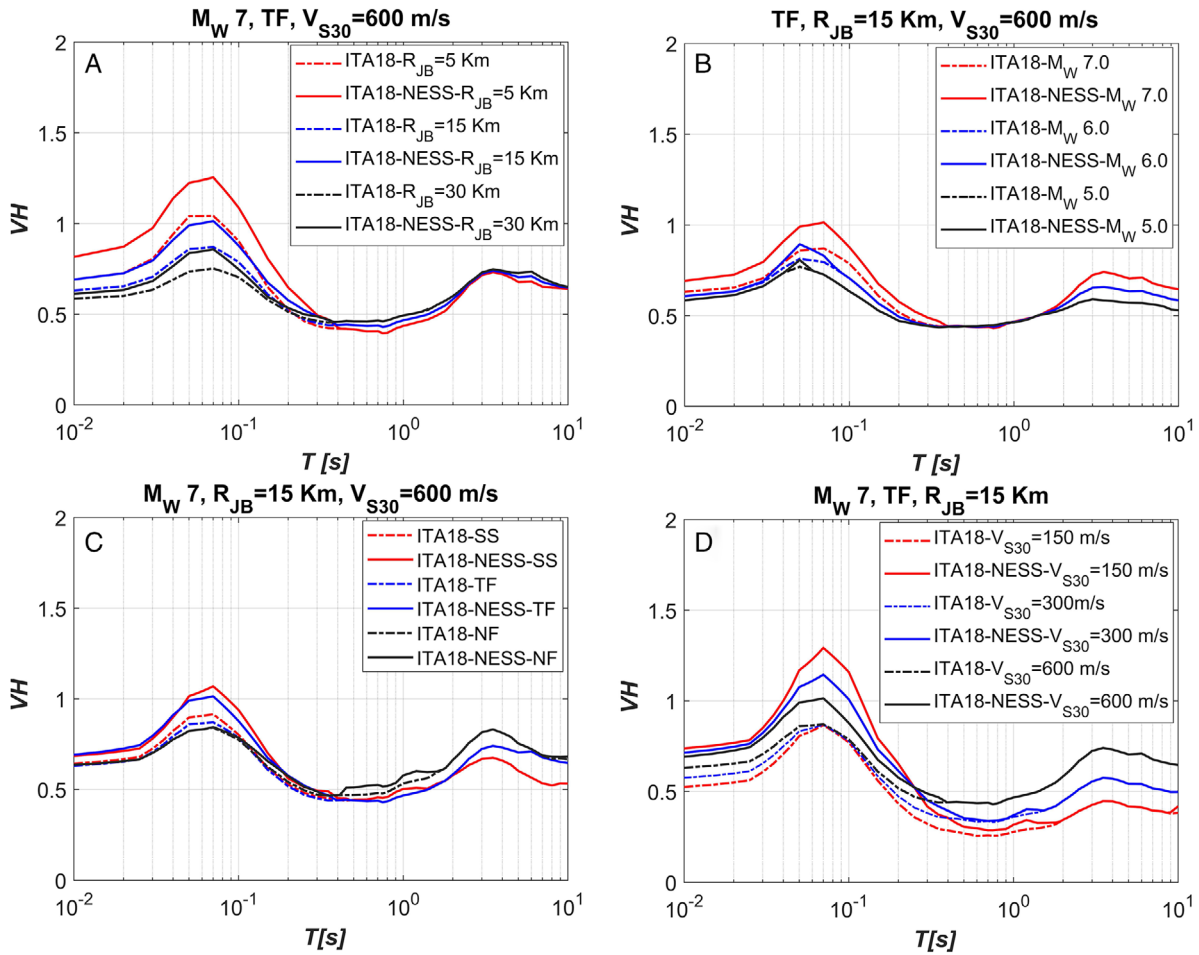


FIGURE 12 Dependence of ITA18 and ITA18-NESS VH median spectra on (A) R_{JB} , (B) M_W , (C) SoF and (D) V_{S30}

Furthermore, as regards the SoF , the correction factor introduces a stronger correlation with the focal mechanism (which was not detected in the ITA18 model), with larger VH ratios for TF and SS compared to NF, which appears to be sound from a physical point of view. With respect to soil condition (Figure 12D), contrary to the ITA18 model, the ITA18-NESS model shows a stronger dependence on soil condition (V_{S30}), yielding, at short periods, to larger ratios for softer sites. In general, it turns out that the model predictions are comparable and the dependence on the explanatory variables tends to be preserved for M_W and reversed for R_{JB} , SoF and V_{S30} in the long period range, but with lower variability. However, it should be considered that in the period range, above around 1 s, VH ratios tend to stabilize around an average value of 2/3.

8 | COMPARISON WITH OTHER STUDIES

Figure 13 shows the comparison of VH spectra from ITA18 and ITA18-NESS models with other GMMs namely, BO2011, GA2011, AK2014 and BC2016 (see Table 1), for $M_W 6.5$ scenarios (TF) at both short (Figure 13A-C-E: $R_{JB} = 5$ km) and large (Figure 13B-D-F: $R_{JB} = 50$ km) distances and for different soil conditions (Figure 13A-B: $V_{S30} = 800$ m/s; Figure 13C-D: $V_{S30} = 400$ m/s; Figure 13E-F: $V_{S30} = 200$ m/s). To estimate the unknown variables, the procedure of Kaklamanos et al.⁵² is applied: assuming a dip angle $\delta = 40^\circ$ and a hanging-wall site, for $M_W 6.5$, $R_{JB} = 5$ (50) km corresponds to R_{rup} of about 10 (52) km. For BC2016, other variables are considered as the default values suggested by the model itself.

At large distance ($R_{JB} = 50$ km) and for rock/stiff site conditions (Figure 13B-D), the models show comparable results, while some differences become appreciable for soft soil site (Figure 13F), for which GA2011, BC2016 and ITA18-NESS show a limited amplification with respect to other models. At short distance ($R_{JB} = 5$ km) and soft sites, the spread of the GMM predictions is significant due to the different modeling assumptions for linear (our models and BO2011) and non-linear

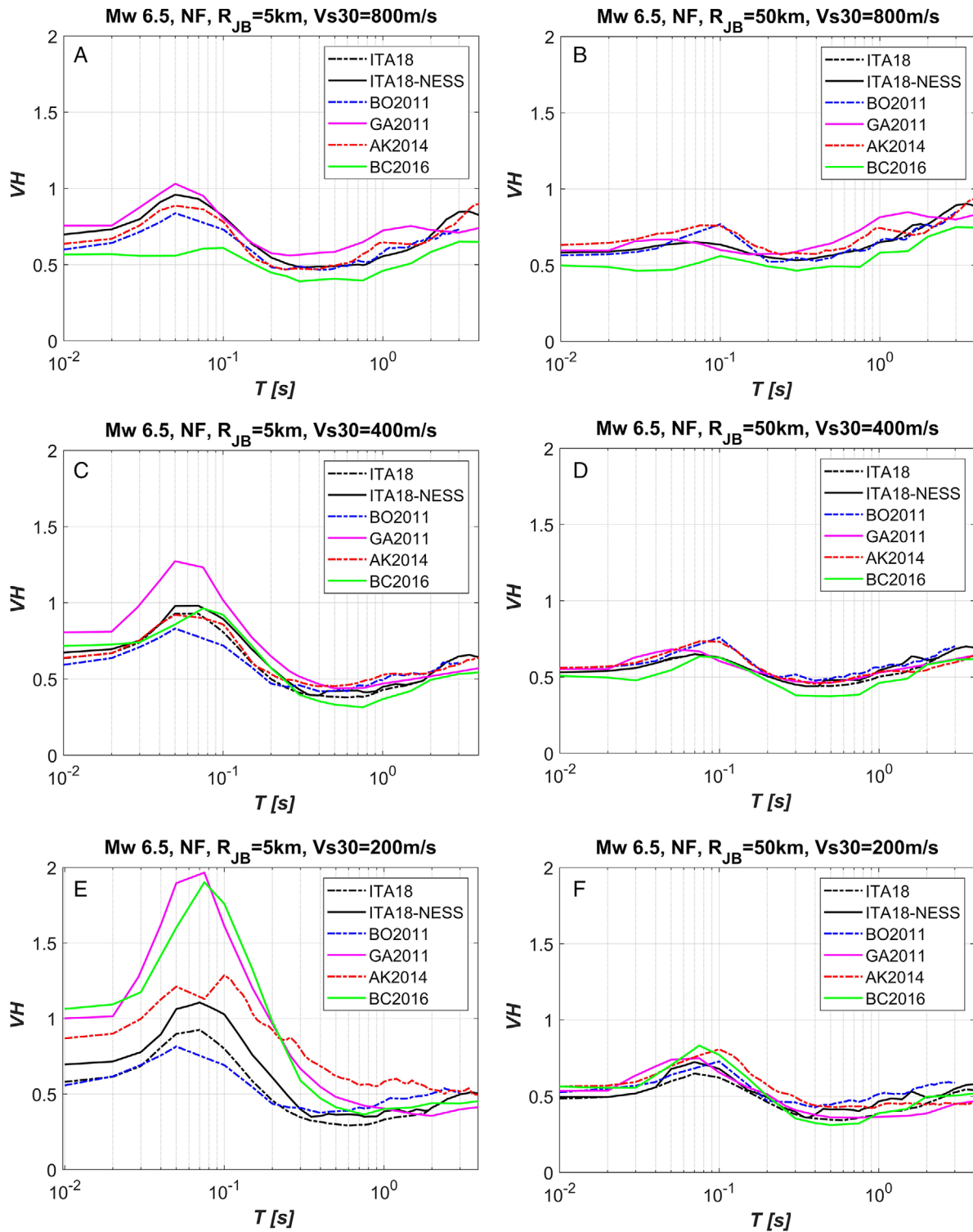


FIGURE 13 Comparison of the proposed VH models with the ones available in the literature (see Table 1), for a reference NF scenario with M_w 6.5 at (A, C, E) R_{JB} = 5 km and (B, D, F) R_{JB} = 50 km, for (A, B) V_{S30} = 800 m/s, (C, D) V_{S30} = 400 m/s and (E, F) V_{S30} = 200 m/s

(GA2011, AK2014 and BC2016) models. In general, at short distances, ITA18-NESS predictions are in broad agreement with GA2011, although the latter provides higher values at soft sites most likely owing to the non-linear site response terms. On the other hand, the ITA18 model tends to be in more agreement with BO2011, owing to the similarity of the seismotectonic context.

9 | CONCLUSIONS

This study presents an empirical GMM for VH response spectral accelerations (up to 10 s), PGA and PGV for shallow crustal earthquakes in Italy. The proposed model is based on the same dataset as for Lanzano et al.,²⁸ i.e. ITA18, and its predictions in near-source conditions are enhanced by the inclusion of an adjustment factor F_{ns} , calibrated using the near-source strong motion dataset NESS. It is worth highlighting that the compatibility of the VH and H models is ensured also with regards to the near-source adjustment. Indeed, a near-source correction factor has been proposed by Sgobba et al.⁵³ also for the horizontal component of Lanzano et al.,²⁸ using the same approach and datasets used in this work. Thus, the VH model can be used in conjunction with the model by Lanzano et al.²⁸ and the adjusted near-source model by Sgobba et al.,⁵³ to derive vertical response spectra compatible with the horizontal ones.

The near-source factor allows for improving the prediction capability of a regional model calibrated solely on the ITA18 dataset, which is poorly constrained in the proximity of the earthquake source, and, therefore, it helps preventing biases in ground motion modeling when moderate-to-strong events and short epicentral distances control the hazard at a site. Although more sophisticated approaches should be grounded on the modeling and parametrization of the physical processes which govern near-source ground motion, the calibration of F_{ns} is regarded as a simplified but effective approach suitable for engineering applications.

Vertical predictions of the proposed model, with and without the near-source adjustment factor, are verified against the available observations from both ITA18 and NESS datasets for selected scenarios, confirming a good predictive capacity of the model. The near-source adjustment is found to be significant especially at distances less than 10 km and for M_W larger than 6.5.

The comparison with independent empirical GMMs shows a comparable behavior both in terms of median estimates, especially for rock and stiff soil sites, and of total variability. However, for very soft sites, the empirical models accounting for non-linear site response exhibit a higher amplification of VH ratios for large M_W and short distance scenarios. Future improvements could be made to the proposed VH model by performing sensitivity studies on the functional form to quantify the impact of some explanatory terms, such as linear Vs non-linear site amplification term. It should be however remarked that the calibration of non-linear site terms is a difficult task due to scarcity of records from well characterized seismic stations.

Furthermore, we underline that in this study the aspects related to the simultaneous occurrence of horizontal and vertical peak ground motions are not addressed, although they deserve particular attention owing to their potential impact on structural response. In this perspective, the GMM could be extended to a larger portfolio of ground motion intensity measures, including also parameters associated with the time shift between vertical and horizontal components, of potential interest for seismic fragility studies on selected classes of structures.

Presently, in Italy, national seismic hazard maps are developed only for the horizontal ground motion. The availability of a GMM for the VH ratios consistent with the horizontal model²⁸ may be beneficial for PSHA of Italy to derive compatible horizontal and vertical response spectral accelerations for engineering applications. Although this work does not propose a rigorous approach for fully consistent horizontal and vertical hazard spectra, which should account also for the correlation between the vertical and horizontal spectral accelerations (see e.g. Gulerce and Abrahamson 20), it represents a step forward for further improvements for code-based VH spectral ratios. In the most simplified approach, the proposed VH model could be used to scale the horizontal UHS, considering the magnitude and distance coming from the hazard deaggregation. The aspects related to the correlation between the H and V/H components across periods will be explored in future studies.

ACKNOWLEDGEMENTS

This work was funded by the DPC-ReLUIS Project WP18 “Normative contributions related to seismic action” and INGV-DPC agreement B1 2019–2021, with the aim of promoting research activities in the field of seismic hazard in Italy. The authors are grateful to Roberto Paolucci, Carlo Lai, Ali Güney Özcebe and Sara Sgobba for their fruitful remarks. The comments by two anonymous reviewers helped improving the paper and are gratefully acknowledged. Open Access Funding provided by Politecnico di Milano within the CRUI-CARE Agreement.

DATA AVAILABILITY STATEMENT

The ITA18 dataset that supports the findings of this study is available from the corresponding author upon reasonable request. The NESS1.0 dataset is openly available at <http://ness.mi.ingv.it/>.

ORCID

Chiara Smerzini  <https://orcid.org/0000-0003-4357-6934>

REFERENCES

1. CS.LL.PP. - Consiglio Superiore dei Lavori Pubblici Norme Tecniche delle Costruzioni, DM 17 gennaio 2018, Gazzetta Ufficiale della Repubblica Italiana 42 (in Italian), 2018.
2. CEN - European Committee for Standardization Eurocode 8. Design of structures for earthquake resistance - Part 1: General rules, seismic actions and rules for buildings, EN 1998-1, 2004.
3. Elgamel AS, He L. Vertical ground motion records: an overview. *Earthq Eng.* 2004;8(5):663-697.
4. Carydis P, Castiglioni C, Lekkas E, Kostaki I, Lebesis N, Drei A. The Emilia Romagna, May 2012 earthquake sequence. The influence of the vertical earthquake component and related geoscientific and engineering aspects. *Ing Sismica.* 2012:31-58.
5. Fiorentino G, Forte A, Pagano E, et al. Damage patterns in the town of Amatrice after August 24th 2016 Central Italy earthquakes. *Bull Earthq Eng.* 2017;16:1399-1423.
6. Papazoglou A, Elnashai A. Analytical and field evidence of the damaging effect of vertical earthquake ground motion. *Earthq Eng Struct Dyn.* 1996;25:1109-1137.
7. Liberatore D, Doglioni C, Alshawa O, Atzori S, Sorrentino L. Effects of coseismic ground vertical motion on masonry constructions damage during the 2016 Amatrice-Norcia (Central Italy) earthquakes. *Soil Dyn Earthq Eng.* 2019;120:423-435. <https://doi.org/10.1016/j.soildyn.2019.02.015>
8. Di Michele F, Cantagallo C, Spacone E. Effects of the vertical seismic component on seismic performance of an unreinforced masonry structures. *Bull Earthq Eng.* 2020;18:1635-1656.
9. Bovo M, Savoia M. Evaluation of force fluctuations induced by vertical seismic component on reinforced concrete precast structures. *Eng Struct.* 2019;178:70-87.
10. Di Sarno L, Elnashai A, Manfredi G. Assessment of RC columns subjected to horizontal and vertical ground motions recorded during the 2009 L'Aquila (Italy) earthquake. *Eng Struct.* 2011;33:1514-1535.
11. Gülerce Z, Abrahamson NA. Vector-valued probabilistic seismic hazard assessment for the effects of vertical ground motions on the seismic response of highway bridges. *Earthq Spectra.* 2010;26(4):999-1016. <https://doi.org/10.1193/1.3464548>
12. Kunnath SK, Erduran E, Chai YH, Yashinsky M. Effect of near-fault vertical ground motions on seismic response of highway overcrossings. *J Bridge Eng.* 2008;13(3):282-290.
13. Bozorgnia Y, Campbell KW. Vertical ground motion model for PGA, PGV, and linear response spectra using the NGA-West2 database. *Earthq Spectra.* 2019;32(2):979-1004. <https://doi.org/10.1193/072814eqs121m>
14. Chiou BS-J & Youngs RR NGA-West2 ground motion prediction equations for vertical ground motions. PEER Report 2013/24: 127-161.
15. Gülerce Z, Kamai R, Abrahamson NA, Silva WJ. Ground motion prediction equations for the vertical ground motion component based on the NGA-W2 database. *Earthq Spectra.* 2017;33(2):499-528. <https://doi.org/10.1193/121814EQS213M>
16. Çağnan Z, Akkar S, Kale Ö, Sandikkaya A. A model for predicting vertical component peak ground acceleration (PGA), peak ground velocity (PGV), and 5% damped pseudospectral acceleration (PSA) for Europe and the Middle East. *Bull Earthq Eng.* 2017;15:2617-2643.
17. Bozorgnia Y, Campbell KW. Ground motion model for the vertical-to-horizontal (V/H) ratios of PGA, PGV, and response spectra. *Earthq Spectra.* 2016;32(2):951-978. <https://doi.org/10.1193/100614eqs151m>
18. Akkar S, Sandikkaya MA, Ay BÖ. Compatible ground-motion prediction equations for damping scaling factors and vertical-to-horizontal spectral amplitude ratios for the broader Europe region. *Bull Earthq Eng.* 2014;12:517-547.
19. Bommer JJ, Akkar S, Kale Ö. A model for vertical-to-horizontal response spectral ratios for Europe and the Middle East. *Bull Seismol Soc Am.* 2011;101(4):1783-1806.
20. Gülerce Z, Abrahamson NA. Site-specific design spectra for vertical ground motion. *Earthq Spectra.* 2011;27(4):1023-1047. <https://doi.org/10.1193/1.3651317>
21. Laouami N. Vertical ground motion prediction equations and vertical-to-horizontal (V/H) ratios of PGA and PSA for Algeria and surrounding region. *Bull Earthq Eng.* 2019;17(7):3637-3660.
22. Zafarani H, Luzi L, Lanzano G, Soghrat MR. Empirical equations for the prediction of PGA and pseudo spectral accelerations using Iranian strong-motion data. *J Seismol.* 2018;22(1):263-285.
23. Zolfaghari MR, Darzi A. A prediction model for vertical-to-horizontal ratios of PGA, PGV, and 5%-damped response spectra (0.01–10 s) for Iran. *J Seismol.* 2019;23(4):819-837.
24. Bozorgnia Y, Campbell KW. The vertical-to-horizontal response spectral ratio and tentative procedures for developing simplified V/H and vertical design spectra. *Earthq Eng.* 2004;8(02):175-207.
25. Haji-Soltani A, Pezeshk S, Malekmohammadi M, Zandieh A. A study of vertical-to-horizontal ratio of earthquake components in the Gulf Coast Region. *Bull Seismol Soc Am.* 2017;107(5):2055-2066.
26. Poggi V, Edwards B, Fäh D. Development of hazard- and amplification- consistent elastic design spectra. *Soil Dyn Earthq Eng.* 2019;126:105-118. <https://doi.org/10.1016/j.soildyn.2018.03.011>
27. Bazzurro P & Cornell CA Vector-valued probabilistic seismic hazard analysis (VPSHA). Proceedings of the 7th US national conference on Earthquake Engineering, Boston, USA, July 21–25, 2002, pp. 10.
28. Lanzano G, Luzi L, Pacor F, et al. A revised ground-motion prediction model for shallow crustal earthquakes in Italy. *Bull Seismol Soc Am.* 2019;109(2):525-540.

29. Atkinson GM. Ground-motion prediction equations for hawaii from a referenced empirical approach. *Bull Seismol Soc Am.* 2010;100(2):751-761. <https://doi.org/10.1785/0120090098>
30. Atkinson GM. Ground-motion prediction equations for eastern north america from a referenced empirical approach: implications for epistemic uncertainty. *Bull Seismol Soc Am.* 2008;98(3):1304-1318.
31. Pacor F, Felicetta C, Lanzano G, et al. NESS1: a worldwide collection of strong-motion data to investigate near-source effects. *Seismol Res Lett.* 2018;89(6):2299-2313.
32. CEN - European Committee for Standardization Eurocode 8. Design of structures for earthquake resistance - Part 1: General rules, seismic actions and rules for buildings, EN 1998-1, 2018 (Working-Draft).
33. USAEC - United States Atomic Energy Commission Design response spectra for seismic design of nuclear power plants, Regulatory Guide RG 1.60, Atomic Energy Commission, 1973.
34. ASCE/SEI 7-16 Minimum design loads for buildings and other structures American Society of Civil Engineering (ASCE), 2016.
35. National Earthquake Hazards Reduction Program (NEHRP). *Recommended Seismic Provisions for New Buildings and Other Structures (FEMA P-20821)*. Washington, D.C.: Building Seismic Safety Council, 2020.
36. Turkish Building Earthquake Code (TBEC-18). Regulations for Buildings to be constructed in Earthquake Prone Areas, Ankara, Turkey; 2018.
37. Kale Ö, Akkar S. A new formulation for a code-based vertical design spectrum. *Earthq Eng Struct Dyn.* 2020;49:963-980.
38. Elnashai AS, Papazoglou AJ. Procedure and spectra for analysis of RC structures subjected to strong vertical earthquake loads. *J Earthquake Eng.* 1997;1(01):121-155. <https://doi.org/10.1080/13632469708962364>
39. National Earthquake Hazards Reduction Program (NEHRP). *Recommended Seismic Provisions for New Buildings and Other Structures (FEMA P-750)*. Washington, D.C.: Building Seismic Safety Council, 2009.
40. Stewart JP, Boore DM, Seyhan E, Atkinson GM. NGA-West2 equations for predicting vertical-component PGA, PGV, and 5%-damped PSA from Shallow Crustal Earthquakes. *Earthq Spectra.* 2019;32:1005-1031. <https://doi.org/10.1193/072114eqs116m>
41. New Zealand Standards NZS 1170.5:2004, Structural Design Actions Part 5: Earthquake actions – New Zealand, Council of Standards New Zealand. 2004.
42. Boore DM, Campbell KW, Atkinson GM. Determination of stress parameters for eight well-recorded earthquakes in eastern north America. *Bull Seismol Soc Am.* 2010;100(4):1632-1645.
43. Kamai RN, Abrahamson NA, Silva WJ. Nonlinear horizontal site amplification for constraining the NGA-West2 GMPEs. *Earthq Spectra.* 2014;30(3):1223-1240. <https://doi.org/10.1193/070113EQS187M>
44. Loviknes K, Kotha SR, Cotton F, Schorlemmer D. Testing nonlinear amplification factors of ground-motion models. *Bull Seismol Soc Am.* 2021;111:2121-2137.
45. Paolucci R, Aimar M, Ciancimino A, et al. Checking the site categorization criteria and amplification factors of the 2020 draft of Eurocode 8 Part 1-1. *Bull Earthq Eng.* 2021;19:4199-4234.
46. Bates D, Mächler M, Bolker B, Walker S. Fitting linear mixed-effects models using lme4. *Jf Stat Softw.* 2015;67(1):1-48.
47. Al Atik L, Abrahamson N, Bommer JJ, Scherbaum F, Cotton F, Kuehn N. The variability of ground-motion prediction models and its components. *Seismol Res Lett.* 2010;81(5):794-801. <https://doi.org/10.1785/gssrl.81.5.794>
48. Wasserstein RL, Lazar NA. The ASA statement on p-values: context, process, and purpose. *Am Stat.* 2016;70(2):129-133.
49. Rodriguez-Marek A, Rathje EM, Bommer JJ, Scherbaum F, Stafford PJ. Application of single-station sigma and site-response characterization in a probabilistic seismic-hazard analysis for a new nuclear site. *Bull Seismol Soc Am.* 2014;104(4):1601-1619.
50. Wald DJ, Allen TI. Topographic slope as a proxy for seismic site conditions and amplification. *Bull Seismol Soc Am.* 2007;97(5):1379-1395.
51. Laurendeau A, Cotton F, Ktenidou O-J, Bonilla LF, Hollender F. Rock and Stiff-Soil Site Amplification: dependency on VS30 and Kappa (κ_0). *Bull Seismol Soc Am.* 2013;103(6):3131-3148.
52. Kaklamanos J, Baise LG, Boore DM. Estimating unknown input parameters when implementing the nga ground-motion prediction equations in engineering practice. *Earthq Spectra.* 2011;27(4):1219-1235. <https://doi.org/10.1193/1.3650372>
53. Sgobba S, Felicetta C, Lanzano G, Ramadan F, D'Amico M, Pacor F. NESS2.0: an updated version of the worldwide dataset for calibrating and adjusting 2 ground-motion models in near-source. *Bull Seismol Soc Am.* 2021.

SUPPORTING INFORMATION

Additional supporting information may be found in the online version of the article at the publisher's website.

How to cite this article: Ramadan F, Smerzini C, Lanzano G, Pacor F. An empirical model for the vertical-to-horizontal spectral ratios for Italy. *Earthquake Engng Struct Dyn.* 2021;1-21. <https://doi.org/10.1002/eqe.3548>

APPENDIX A

TABLE A.1 Main parameters for the definition of the vertical design spectrum (for a reference damping ratio of 5%) according to different seismic norms, namely: EC8, EC8-Draft, NTC18, ASCE 7–16, NEHRP 2020 and TBEC18

Seismic Norm	Main parameters for the definition of the vertical 5%-damped design spectrum	Assumed values for Figure 2
EC8	$S_{ve}(T) = f(PGA_v, T_{Bv}, T_{Cv}, T_{Dv})$ PGA_v = vertical peak ground acceleration defined as a ratio of the horizontal counterpart PGA: $PGA_v/PGA = 0.9$ for Type 1 spectrum ($M_S \geq 5.5$) $PGA_v/PGA = 0.45$ for Type 2 spectrum ($M_S < 5.5$) T_{Bv}, T_{Cv}, T_{Dv} = vertical corner periods marking the beginning of constant acceleration, constant velocity and constant displacement branch, respectively: $T_{Bv} = 0.05$ s, $T_{Cv} = 0.15$ s, $T_{Dv} = 1.0$ s for both Type 1 and 2	Type 1 spectrum
EC8-Draft	$S_{ve}(T) = f(S_{av}, S_{\beta v}, T_{Bv}, T_{Cv}, T_{Dv})$ S_{av} = maximum response spectral acceleration corresponding to the constant acceleration range defined as a function of horizontal counterpart S_α : $S_{av} = f_{vh\alpha} \cdot S_\alpha$ with $f_{vh\alpha} = \begin{cases} 0.6 & \text{if } S_\alpha < 2.5 \text{ m/s}^2 \\ 0.04 \cdot S_\alpha + 0.5 & \text{if } 2.5 \text{ m/s}^2 \leq S_\alpha \leq 7.5 \text{ m/s}^2 \\ 0.8 & \text{if } S_\alpha > 7.5 \text{ m/s}^2 \end{cases}$ $S_{\beta v}$ = maximum response spectral acceleration at $T_\beta = 1$ s defined as a function of horizontal counterpart S_β : $S_{\beta v} = f_{vh\beta} \cdot S_\beta$ with $f_{vh\beta} = 0.6$ $T_{Bv} = 0.05$ s, $T_{Cv} = \frac{S_{\beta v} \cdot T_\beta}{S_{av}}$, $T_{Dv} = T_D$ (horizontal)	Values of S_α and S_β for reference rock site category: $S_{\alpha,ref} = 7.5 \text{ m/s}^2$ $S_{\beta,ref} = 3 \text{ m/s}^2$
NTC18	$S_{ve}(T) = f(PGA, F_v, T_{Bv}, T_{Cv}, T_{Dv})$ F_v : factor quantifying the maximum spectral acceleration as a function of horizontal PGA and F_0 (factor for maximum spectral amplification ≥ 2.2) $F_v = 1.35 \cdot F_0 \cdot \left(\frac{PGA}{g}\right)^{0.5}$ $T_{Bv} = 0.05$ s, $T_{Cv} = 0.15$ s, $T_{Dv} = 1.0$ s	Base hazard parameters for reference rock site category $PGA = 2.0 \text{ m/s}^2$ $F_0 = 2.41$ $T_C^* = 0.375$
ASCE 7–16 (NEHRP 2009)	$S_{ve}(T) = f(S_{DS}, C_v, T_{Bv}, T_{Cv}, T_{Dv})$ S_{DS} = design response spectral acceleration at short periods C_v = vertical coefficient defined as a function of site classes and of S_S , which is the mapped Maximum Credible Earthquake (MCE) response spectral acceleration at short periods T_{Av} (short period cut-off) = 0.025 s, $T_{Bv} = 0.05$ s, $T_{Cv} = 0.15$ s, $T_{Dv} = 2.0$ s	MCE response spectral acceleration at short periods and at 1 s: $S_S = 1.7$ g $S_1 = 0.7$ g
NEHRP 2020	$S_{ve}(T) = f(S_a, C_v, F_{md}, T_{Bv}, T_{Cv}, T_{Dv})$ S_a = design response spectral acceleration at the same period T as for the vertical spectrum C_v = vertical coefficient defined as a function of site classes and of S_{MS} , which is the MCE response spectral acceleration at short periods F_{md} = period-dependent factor to convert the median-component spectral ordinate to a maximum direction spectral ordinate $T_{Av} = 0.025$ s, $T_{Bv} = 0.05$ s, $T_{Cv} = 0.1$ s, $T_{Dv} = 2.0$ s	$S_S = 1.7$ g $S_1 = 0.7$ g
TBEC18	$S_{ve}(T) = f(S_{DS}, T_{Bv}, T_{Cv}, T_{Dv})$ S_{DS} = design response spectral acceleration at short periods $T_{Bv} = T_B/3$, $T_{Cv} = T_C/3$, $T_{Dv} = T_D/2$, where T_B, T_C and T_D are the horizontal corner periods	$S_S = 1.7$ g $S_1 = 0.7$ g